Science Press

ARTICLE

Microstructure and Properties of High Strength Tantalum Prepared by Selective Electron Beam Melting

Yang Kun,   Wang Jian,   Yang Guangyu,   Liu Nan,   Jia Liang

State Key Laboratory of Porous Metal Materials, Northwest Institute for Nonferrous Metal Research, Xi`an 710016, China

Abstract: Bulk tantalum specimens of high relative density (99.93%) without obvious defects were prepared by powder bed selective electron beam melting (SEBM) process, and their microstructure as well as mechanical properties were investigated. Results show that the as-deposited tantalum specimens have strong columnar grain structures parallel to the building direction. The strong (001) texture and a large number of low-angle grain boundaries can be observed in the bulk specimens due to the extremely high cooling rate during additive manufacturing. Because of the solid solution strength of interstitial oxygen and nitrogen elements, the as-SEBMed tantalum specimens exhibit excellent room-temperature yield strength of 613.55±2.57 MPa and outstanding elongation of 30.55%±4.23%.

Key words: additive manufacturing; tantalum; selective electron beam melting; mechanical properties

Tantalum is a refractory metal with excellent properties, including excellent corrosion resistance, superior electrical properties, and good biocompatibility[1–2]. Different from tungsten and molybdenum, tantalum exhibits excellent ductility at room temperature. Based on these characteristics, tantalum has been widely used in aerospace, orthopedic implants, and chemical engineering[3–5]. However, since the melting point of tantalum is close to 3000 °C, the tantalum parts are usually manufactured by powder metallurgy (PM) and electron beam (EB) melting techniques, resulting in high cost and long production time, particularly for the manufacture of complex parts[6–8].

Currently, the additive manufacturing technique, including selective laser melting (SLM), selective electron beam melting (SEBM), and laser melting deposition (LMD), attracts much attention as a rapid and personalized manufacture method for the tantalum components[9–11]. Fox et al[12] fabricated the porous tantalum specimens by SLM for biomedical application. Zhou[13] and Shi[14] et al studied the microstructure and mechanical properties of SLMed tantalum before and after heat treatment. Furthermore, Guan et al[15] investigated the evolution of porosity, microstructure, hardness, and tensile mechanical properties of LMD-treated tantalum. It is reported that the mechanical properties of tantalum specimens prepared by additive manufacture are quite different from those prepared by traditional methods. The yield strength of SLMed tantalum specimens is 285–601 MPa, and their elongation fluctuates in the range of 2%–35%[12,16–17].

Based on the powder bed additive manufacturing technique, SEBM process has the advantages of high-energy density, high producing rate, and high vacuum building environment[18]. Due to the high scanning speed of electron beam, the powder bed is usually preheated and kept at 1200 °C to prevent the crack formation and release thermal stress[19]. It is found that SEBM is very suitable for the near-net-shape formation of refractory metal and brittle metal components[20–23]. Tang et al[22] reported that the custom-designed tantalum implants can be achieved by SEBM. Guo et al[24] focused on the effects of reuse on the properties of tantalum powders and tantalum parts. However, the microstructure evolution and mechanical performance of SEBMed bulk tantalum are rarely investigated, which restricts the application of SEBM treatment for refractory metals.

In this research, the bulk tantalum specimens were fabricated by SEBM process, and the microstructure evolution, mechanical properties, and strengthening mechanism were analyzed.

1 Experiment

The spherical tantalum powder was fabricated by plasma spheroidization process, and its morphology is shown in Fig.1. The average particle size of the tantalum powder is 14.9 μm, which is much smaller than that in Ref.[22]. The properties and the chemical composition of tantalum powder are listed in Table 1 and Table 2, respectively.

All the tantalum specimens (*Φ*10 mm×50 mm) were fabricated through SEBM equipment (Sailong S2, Xi'an Sailong Metal Materials Co., Ltd). The processing parameters were as follows: voltage=60 kV; beam current=11.2 mA; scanning speed=120 mm/s during the melting process[19,21]. The layer thickness was 50 μm and the hatch distance was 100 μm. The vacuum pressure was lower than 10^{-2} Pa. Therefore, the pick-up of interstitial elements during the manufacturing process could be neglected. The substrate temperature during SEBM process was monitored by a thermal couple attached to the substrate bottom, and the recorded temperature variation is shown in Fig.2. The preheating temperature was 950 °C and then it was kept at about 1020 °C over 30 h for SEBM process.
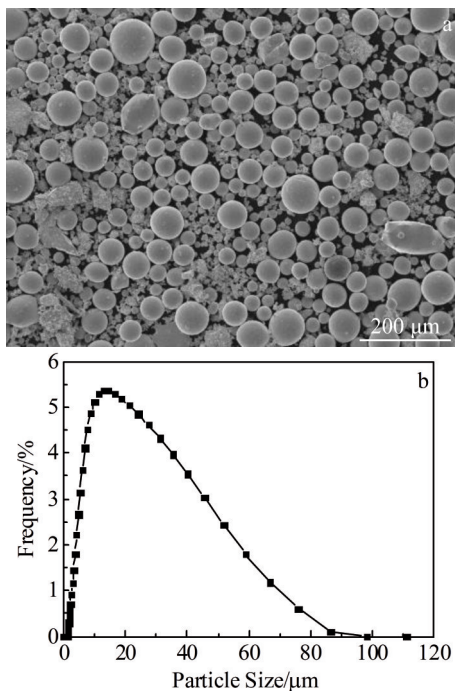
Fig.1 Morphology (a) and particle size distribution (b) of spherical tantalum powder prepared for SEBM process

Table 1 Properties of spherical tantalum powder prepared for SEBM process

Particle size/μm			Flowability/	Apparent	Tap density/
D_{10}	D_{50}	D_{90}	s·(50 g)$^{-1}$	density/g·cm^{-3}	g·cm^{-3}
4.62	14.9	44.2	13.83	5.23	7.99

Table 2 Chemical composition of tantalum powder (wt%)

C	O	N	Nb	Fe	W	Mo	Ta
0.0015	0.1100	0.0049	0.0003	0.0027	0.0010	0.0015	Bal.
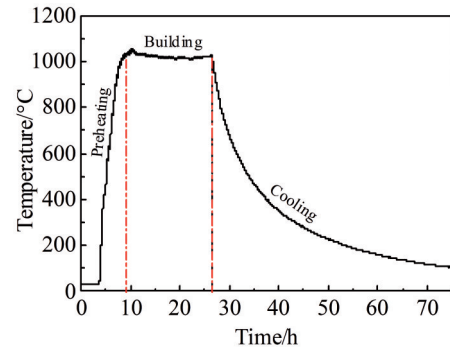
Fig.2 Temperature variation of substrate during SEBM process

The density of as-built dense tantalum specimens was measured by Archimedes method. The theoretical density of pure tantalum is 16.69 g/cm^3 [25]. X-ray diffraction (XRD) analysis was performed by Bruker D8 Advance diffractometer at 40 kV with Cu Kα radiation (wavelength *λ*=0.154 060 nm). The specimens selected for optical microscope (OM) observation were cut along the building direction and mechanically ground followed by polishing treatment. Then, they were etched by mixed solution of 10 mL HF, 10 mL HNO$_3$, and 30 mL H$_2$SO$_4$. The microstructure and phase components of the tantalum specimens were further examined by transmission electron microscope (TEM, JEM 200CX) and selected area electron diffraction (SAED) at 120 kV. Electron backscattered scanning diffraction (EBSD) measurement was operated at 20 kV and performed on an area of 1 mm×1 mm with step size of 0.8 μm. The data processing was completed by HKL-EBSD Channel 5 software. The areas between grains were classified as low-angle grain boundaries (LAGBs) when the misorientation angle was between 2° and 15°; when the misorientation angle was above 15°, the areas were regarded as high-angle grain boundaries (HAGBs).

The specimens for tensile tests were prepared according to ASTM E8/E8M-16a standard, and the tensile test was performed at room temperature by Instron 5982 machine at strain rate of 10^{-3} s^{-1}. Three specimens were tested and the standard deviations were obtained. The fracture morphologies of SEBMed Ta specimens were analyzed by scanning electron microscope (SEM, JEOL JMS-6700 F, Japan).

2 Results

2.1 Phase identification and microstructure evolution

XRD patterns of the raw tantalum powder and as-built bulk specimens are shown in Fig.3. It is found that all peaks are related to the Ta phase of body-centered cubic structure, and no other peaks can be observed. Besides, the obvious intensity difference between raw Ta powder and bulk Ta specimen suggests that the crystallographic texture exists in the bulk Ta specimen[26].

The representative microstructure of bulk tantalum specimen is shown in Fig.4. A few insufficiently diffused defects can be observed, and the relative density of the bulk tantalum specimens is 99.93%. The columnar grains grow due
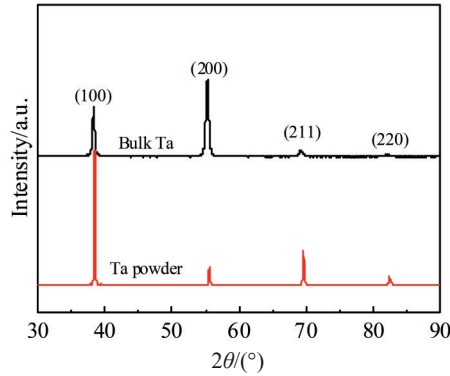
Fig.3   XRD patterns of raw Ta powder and as-built bulk Ta specimen
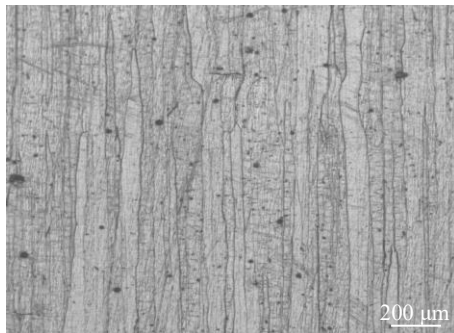
Fig.4   Microstructure of bulk Ta specimen

to the high-temperature gradient along the building direction during SEBM process, and the average width of columnar grains is 53.15±21.88 μm. Different from that of SLMed tantalum[13], the growth direction of columnar grains in SEBMed tantalum specimens is almost parallel to the building direction. In addition, the width of columnar grains is smaller than that fabricated by SLM[13] and wire+arc additive

manufacturing (WAAM)[27]. These phenomena are mainly attributed to the fine powder and high powder temperature, which results in the low thermal gradient at the solid/liquid interface of pool boundaries[13,28].

EBSD maps of grain boundary and grain structure in bulk tantalum specimen along the building direction are shown in Fig. 5. Generally, the as-built tantalum specimen exhibits the strong (001) texture, which is attributed to the heat flow through the building platform. As shown in Fig. 5c, the blue lines represent LAGBs ($\theta = 2° - 15°$); the red lines represent HAGBs ($\theta > 15°$). Obviously, LAGBs are in dominant position (70.79%), which is mainly due to the large temperature gradient[29].

2.2 Mechanical properties

The room-temperature tensile tests were conducted on the as-built Ta specimens along the building direction of pure tantalum specimens, and the stress-strain curves are shown in Fig. 6. The tensile properties of Ta specimens prepared by different processes are summarized in Table 3.

SEBMed tantalum specimens exhibit excellent yield strength (613.55±2.57 MPa) and ultimate tensile strength (649.92±3.16 MPa). Additionally, SEBMed tantalum specimens have the excellent ductility (30.55%±4.23%), which is comparable to that of PMed tantalum with low oxygen content.

The fracture surfaces of Ta specimen are shown in Fig. 7. It can be seen that the fracture surface presents the characteristics of ductile fracture: a cup morphology can be observed and the shear lips exist around the periphery of tension bar, as shown in Fig. 7a. Moreover, the necking phenomenon occurs: the fracture surface area shrinks by approximately 20%, compared with the initial cross-section area. As shown in Fig. 7b, a large number of dimples do not appear. Instead, a series of voids and ductile dimples appear
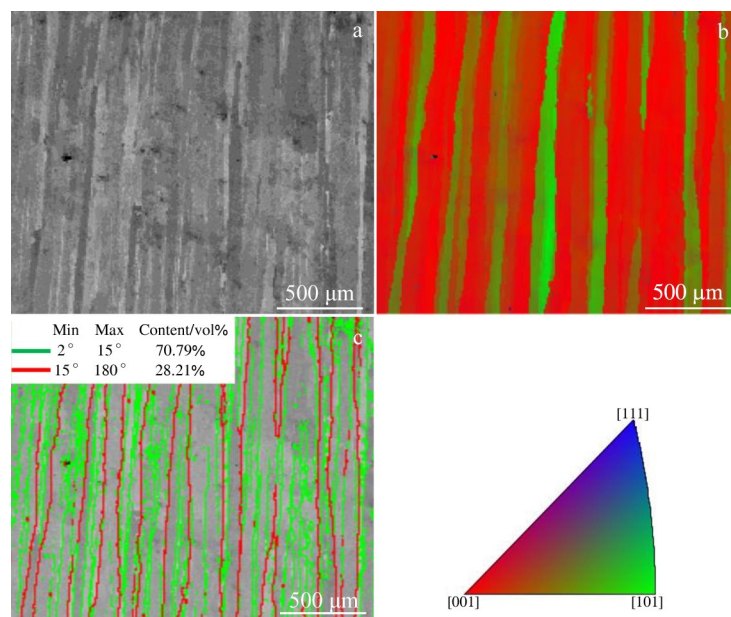
Fig.5   SEM microstructure (a), EBSD grain boundary map (b), and EBSD grain structure map (c) of as-built Ta specimen along building direction
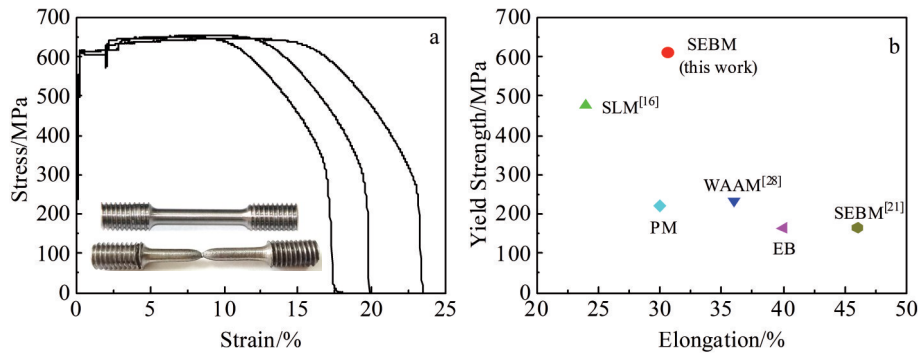
Fig.6 Stress-strain curves of bulk Ta specimens prepared by SEBM process (a); relationships between yield strength and elongation of Ta specimens prepared by different processes (b)

on the fracture surface with size of 2–50 μm.

To further analyze the fracture behavior, the tensile specimen was cut along the cross-sectional fracture surface, as shown in Fig. 8. It can be clearly seen that the necking phenomenon is obvious, and the columnar grains are severely elongated and distorted in the necking region. The fracture surface has a concave shape with jagged sawtooth morphology, which is consistent with the fracture morphologies containing voids and ductile dimples (Fig. 7b). In addition, several enlarged cavities are distributed near the necking region. Based on the abovementioned discussion, it can be inferred that the fracture process of SEBMed tantalum specimen obeys the traditional nucleation-growth-coalescence process of void[5]: the fracture starts from the cavities in the specimen center, and then expands to the specimen edge. Moreover, as a pure metal specimen, the void may be nucleated at specific sub-grain configurations[5] and pore

defects during SEBM process, which should be further investigated.

3 Discussion

Based on the abovementioned results, it can be concluded that the bulk tantalum specimens with high relative density can be fabricated by SEBM process. The SEBMed tantalum has superior yield strength and comparable elongation. Normally, the strengthening methods of polycrystalline metal mainly include the precipitation hardening, grain-boundary hardening, solid-solution hardening, and dislocation hardening[30]. The improved yield strength $\sigma_{0.2}$ can be expressed by Eq.(1), as follows:

$$\sigma_{0.2}=\sigma_0+\Delta\sigma_p+\Delta\sigma_g+\Delta\sigma_s+\Delta\sigma_d \qquad (1)$$

where σ_0 is the theoretical intrinsic strength of tantalum (68.6 MPa) [31]; σ_p, σ_g, σ_s, and σ_d are the individual strengthening

Table 3 Mechanical properties of Ta specimens prepared by different processes

Method	O content/wt%	Yield strength/MPa	Ultimate tensile strength/MPa	Elongation/%	Ref.
SEBM	0.110	613.55±2.57	649.92±3.16	30.55±4.23	This work
SLM	0.150	Approximately 550	Approximately 600	Approximately 1.7	[13]
SLM	0.044	477	544	24	[16]
SEBM	0.009	261±13	326±3	46±1	[22]
WAAM	0.0266	234±10	261±3	36±6	[27]
PM	≤0.030	220	310	30	[27]
EB	≤0.015	165	205	40	[27]
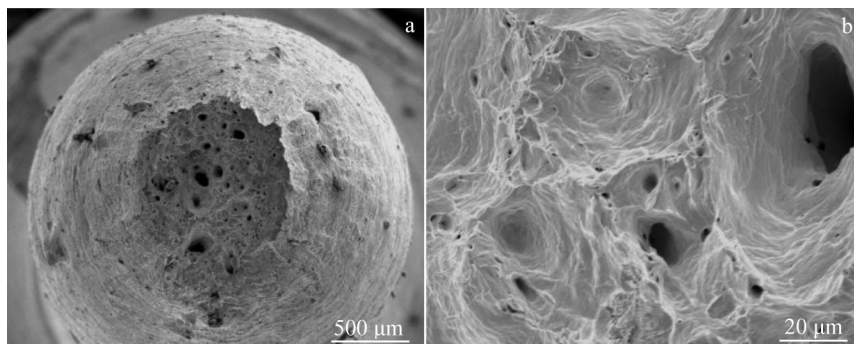
Fig.7 Fracture surfaces of tantalum specimen at low (a) and high (b) magnifications
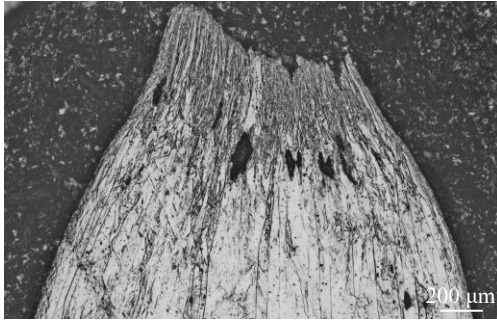
Fig.8 OM cross-sectional morphology of Ta specimen after tensile fracture

contributions of the precipitation hardening, grain-boundary hardening, solid-solution hardening, and dislocation hardening methods, respectively.

3.1 Precipitation hardening

According to the experiment results, no precipitation, such as Ta_2O_5, can be observed in the bulk tantalum specimen. To confirm this conclusion, TEM image and corresponding SAED pattern of tantalum specimen are shown in Fig.9.

Still, no precipitation can be observed, indicating that the high vacuum protection during SEBM process protects the tantalum powder away from interstitial elements. Therefore, it can be inferred that the contribution of precipitation strengthening is negligible for the as-built tantalum specimens.

3.2 Solid-solution hardening

It is well known that the mechanical properties of bulk tantalum are sensitive to the interstitial elements[7]. Therefore, the strengthening effect of oxygen and nitrogen should be considered. Puhr-Westerheide et al[31] established a relationship between strength and interstitial element content, and the solution strengthening contribution $\Delta\sigma_s$ can be expressed by Eq.(2), as follows:

$$\Delta\sigma_s = 123.5 + 676.2C_N + 392\,C_O \tag{2}$$

where C_N and C_O are the atomic percentage of nitrogen and oxygen in tantalum, respectively. The contents of O and N interstitial elements in SEBMed tantalum specimens are 1.11at% and 0.01at%, respectively. Therefore, σ_s for the bulk tantalum is calculated as 569.8 MPa.
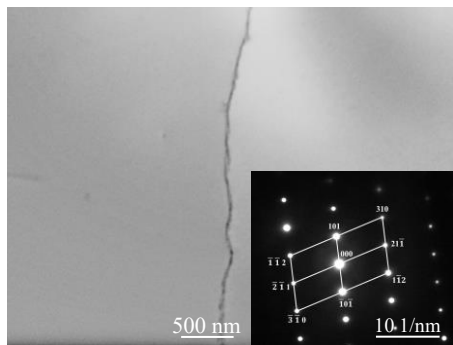
3.3 Grain-boundary hardening

Small grain size results in the high volume fraction of grain boundaries, which impede the dislocation motion. The relationship between yield strength and grain size can be described by the classical Hall-Petch equation, as follows:

$$\Delta\sigma_g = k_y(d_{SEBN}^{-1/2} - d_a^{-1/2}) \tag{3}$$

where k_y is the strengthening coefficient for tantalum (3.03 MPa/mm^2 [32]); d_{SEBM} and d_a represent the average grain diameter of SEBMed tantalum (53.15±21.8 μm) and as-forged tantalum (approximately 70 μm[33]), respectively. Therefore, the corresponding $\Delta\sigma_g$ is only 4 MPa. This result indicates that the strengthening contribution of the grain-boundary hardening is very limited.

3.4 Dislocation hardening

It is reported that the dislocation strengthening is an important method to improve the mechanical properties of metals prepared by additive manufacturing, such as stainless steel[34], copper[35], and pure titanium[36]. Therefore, the Bailey-Hirsch formula[30] can be used to calculate the strengthening effect of the dislocation, as follows:

$$\Delta\sigma_d = 3.8M\alpha G\varepsilon \tag{4}$$

where M and α are the constants for tantalum; G is the shear modulus for tantalum; ε is the micro-strain caused by dislocations. According to the Williamson-Hall method[30,36], the micro-strain ε is determined by the linear fitting slope of $\beta\cos\theta$-$4\sin\theta$ plot, where β is XRD peak broadening position and θ is Bragg angel of certain peak.

The results are shown in Fig. 10. It can be seen that the micro-stain of bulk tantalum specimen is nearly zero (0.04), indicating that the dislocation strengthening $\Delta\sigma_d \approx 0$. The calculation results agree well with the observation results by TEM analysis (Fig. 9). This is because the temperature of powder bed (1020 °C) is close to the stress-release temperature of tantalum[37], and the duration for in-situ annealing in SEBM process is sufficient to annihilate the dislocations and release the residual stress[38]. Therefore, the dislocation hardening has a little effect on the strength enhancement.

Therefore, it can be concluded that the calculated yield strength of bulk tantalum is 678.4 MPa, which is consistent with the experimental value (613.55 MPa). It is apparent that

Fig.9 TEM image and corresponding SAED pattern of bulk tantalum specimen prepared by SEBM process
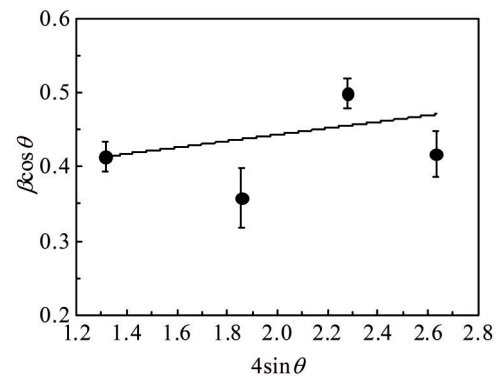
Fig.10 $\beta\cos\theta$-$4\sin\theta$ data and corresponding fitting line of bulk Ta specimen

the solid-solution strengthening of interstitial elements is dominant in the strength enhancement of SEBMed bulk tantalum specimen. Consequently, SEBM process is an effective method to produce bulk tantalum with excellent strength and high ductility.

4 Conclusions

1) The microstructure of tantalum specimens prepared by selective electron beam melting (SEBM) process consists of fine columnar grains parallel to the building direction. Fast cooling rate results in the formation of the strong (001) texture and a large number of low-angle grain boundaries in the bulk tantalum specimens.

2) No precipitates or dislocations can be observed in the SEBMed tantalum specimens, which is mainly attributed to the high vacuum building environment and in-situ heat treatment during SEBM process.

3) The tantalum specimen prepared by SEBM process exhibits excellent yield strength of 613.55±2.57 MPa, ultimate tensile strength of 649.92±3.16 MPa, and outstanding elongation of 30.55%±4.23%, which are basically better than those of the bulk tantalum prepared by other traditional methods. The improved yield strength is mainly attributed to the solid-solution strengthening of interstitial elements.

References

1 Dong C, Bi X L, Yu J G *et al. Journal of Alloys and Compounds*[J], 2019, 781: 84

2 Yang Kun, Wang Jian, Tang Huiping *et al. Rare Metal Materials and Engineering*[J], 2022, 51(10): 3922 (in Chinese)

3 Levine B R, Sporer S, Poggie R A *et al. Biomaterials*[J], 2006, 27(27): 4671

4 Efe M, Kim H J, Chandrasekar S *et al. Materials Science and Engineering A*[J], 2012, 544: 1

5 Zhao D L, Liang H, Han C J *et al. Additive Manufacturing*[J], 2021, 47: 102 223

6 Köck W, Paschen P. *JOM*[J], 1989, 41(10): 33

7 Cardonne S M, Kumar P, Michaluk C A *et al. International Journal of Refractory Metals and Hard Materials*[J], 1995, 13(4): 187

8 Zhao D L, Han C J, Li Y *et al. Journal of Alloys and Compounds*[J], 2019, 804: 288

9 Qian H, Lei T, Lei P F *et al. Tissue Engineering Part B: Reviews*[J], 2020, 27(2): 166

10 Gao H R, Yang J Z, Jin X *et al. Materials & Design*[J], 2021, 210: 110 095

11 Jafarlou D M, Sousa B C, Gleason M A *et al. Additive Manufacturing*[J], 2021, 47: 102 243

12 Fox P, Pogson S, Sutcliffe C J *et al. Surface and Coatings Technology*[J], 2008, 202(20): 5001

13 Zhou L B, Chen J, Li C *et al. Materials Science and Engineering A*[J], 2020, 785: 139 352

14 Shi Q, Mao X H, Tang C *et al. Rare Metal Materials and Engineering*[J], 2020, 49(12): 4023

15 Guan B S, Xu M G, Yang X S *et al. International Journal of Refractory Metals and Hard Materials*[J], 2022, 103: 105 773

16 Zhou L, Yuan T, Li R *et al. Materials Science and Engineering A*[J], 2017, 707: 443

17 Yang J Z, Jin X, Gao H R *et al. Materials Characterization*[J], 2020, 170: 110 694

18 Lu S L, Qian M, Tang H P *et al. Acta Materialia*[J], 2016, 104: 303

19 Yang K, Wang J, Tang H P *et al. Journal of Alloys and Compounds*[J], 2020, 826: 154 178

20 Wang J, Yang K, Liu N *et al. JOM*[J], 2017, 69(12): 2751

21 Yang G, Yang P, Yang K *et al. International Journal of Refractory Metals and Hard Materials*[J], 2019, 84: 105 040

22 Tang H P, Yang K, Jia L *et al. JOM*[J], 2020, 72(3): 1016

23 Yue H, Chen Y, Wang X *et al. Journal of Alloys and Compounds*[J], 2018, 766: 450

24 Guo Y, Chen C, Wang Q B *et al. Materials Research Express*[J], 2021, 8(4): 46 538

25 Lide D R. *CRC Handbook of Chemistry and Physics*[M]. Calabas: CRC Press, 2004

26 Thijs L, Montero S M L, Wauthle R *et al. Acta Materialia*[J], 2013, 61(12): 4657

27 Marinelli G, Martina F, Ganguly S *et al. International Journal of Refractory Metals and Hard Materials*[J], 2019, 83: 104 974

28 De Formanoir C, Michotte S, Rigo O *et al. Materials Science and Engineering A*[J], 2016, 652: 105

29 Ni M, Liu S C, Chen C *et al. Materials Science and Engineering A*[J], 2019, 748: 275

30 Luo X, Liu L H, Yang C *et al. Journal of Materials Science & Technology*[J], 2021, 68: 112

31 Puhr-Westerheide J, Elssner G. *Journal of the Less Common Metals*[J], 1970, 20(4): 371

32 Wright S I, Gray G T, Rollett A D. *Metallurgical and Materials Transactions A*[J], 1994, 25(5): 1025

33 Levin Z S, Wang X, Kaynak M *et al. International Journal of Refractory Metals and Hard Materials*[J], 2019, 80: 73

34 Barkia B, Aubry P, Haghi-Ashtiani P *et al. Journal of Materials Science & Technology*[J], 2020, 41: 209

35 Li Z, Cui Y N, Yan W T *et al. Materials Today*[J], 2021, 50: 79

36 Yamanaka K, Saito W, Mori M *et al. Additive Manufacturing*[J], 2015, 8: 105

37 Goodwin F, Guruswamy S, Kainer K U *et al. Metals*[M]. Heidelberg: Springer, 2005

38 Hrabe N, Gnäupel-Herold T, Quinn T. *International Journal of Fatigue*[J], 2017, 94: 202

电子束选区熔化成形高强钽的组织与性能

杨　坤，王　建，杨广宇，刘　楠，贾　亮

(西北有色金属研究院 金属多孔材料国家重点实验室，陕西 西安 710016)

摘　要： 采用粉末床电子束选区熔化技术制备了高密度（99.93%）且无明显缺陷的块状钽样品，并对其微观结构、力学性能进行了研究。结果表明，沉积态的钽金属具有平行于生长方向的柱状晶结构。由于成形过程中的高冷却速率，在块状样品中观察到（001）织构和大量的小角度晶界。由于间隙元素氧和氮的固溶强化，电子束选区熔化成形的钽试样表现出了优异的室温屈服强度（613.55±2.57 MPa）和延伸率（30.55%±4.23%）。

关键词： 增材制造；钽；电子束选区熔化；力学性能

作者简介：杨　坤，男，1987 年生，博士，教授级高级工程师，西北有色金属研究院金属多孔材料国家重点实验室，陕西 西安 710016，电话：029-86231095，E-mail：yangk029@163.com